Efficient recovery of lithium from the reverse osmosis concentrate of shale gas wastewater treatment: Adsorption performance and mechanism of Al-doped manganese-based

In preparation for ***Desalination***

Date: *Apr 18, 2025*

Efficient recovery of lithium from the reverse osmosis concentrate of shale gas wastewater treatment: Adsorption performance and mechanism of Al-doped manganese-based adsorbent particles prepared via hydrophilic modification.

Xin Li [a,b], Xifan Li [a,b], Quanxun Liang [c], Guijing Chen [a,b], Wenjie Wang [a,b], Jin Bao [d], Jiawang Qin [c], Shun Tang [c], Xiao Lin [e], Alberto Tiraferri [f], Baicang Liu [a, b, *]

[a] State Key Laboratory of Hydraulics and Mountain River Engineering, College of Architecture and Environment, Institute of New Energy and Low-Carbon Technology, Sichuan University, Chengdu, Sichuan 610207, PR China

[b] Yibin Institute of Industrial Technology, Sichuan University Yibin Park, Section 2, Lingang Ave., Cuiping District, Yibin, Sichuan 644000, PR China

[c] China Dongfang Electric Group Co., Ltd, Chengdu, Sichuan 611730, PR China

[d] Chuanqing Drilling Engineering Company Limited, Chinese National Petroleum Corporation, Chengdu, Sichuan 610081, PR China

[e] Botree Cycling Co., Ltd., Suzhou, Jiangsu 215006, PR China

[*]Corresponding author. Tel.: +86-28-85995998; fax: +86-28-62138325; E-mail: bcliu@scu.edu.cn; baicangliu@gmail.com (B. Liu).

[f] Department of Environment, Land and Infrastructure Engineering, Politecnico di Torino, Corso Duca degli Abruzzi 24, 10129 Turin, Italy

Abstract: The growing demand for lithium in energy storage batteries has driven interest in extracting lithium from shale gas wastewater as a sustainable alternative to traditional mining. To address challenges such as high cycling loss of adsorbent powder and complex operational procedures, this study developed adsorbent spheres by pelletizing Al-modified $H_{1.33}Mn_{1.67}O_4$ powder with polyvinyl chloride (PVC) as the skeleton material, and introducing cellulose acetate (CA) or Pluronic F127 as hydrophilic modifiers. CA-modified powder exhibited superior mechanical stability, internal porosity, and hydrophilicity. These properties reduced interference from organic matter and allowed a lithium adsorption capacity of 20.2 mg/g, surpassing the 18.8 mg/g capacity of unmodified PVC particles. Adsorption behavior followed the Freundlich isotherm model, while pseudo-second-order kinetics indicated that multi-step and multi-layer chemisorption governed lithium uptake. In fixed-bed filtration experiments, the optimal empty bed contact time (EBCT) was determined to be 40 minutes, leading to an adsorption saturation bed volume more than 40 times the empty bed volume. Desorption enrichment provided lithium concentrations of approximately 200 mg/L. The adsorbent maintained its adsorption capacity over 10 adsorption-desorption cycles, with manganese dissolution losses below 0.3% and in some cases as low as 0.2%. These findings confirm the durability and efficacy of the novel

composite adsorbent in lithium recovery, offering a significant step toward more efficient and sustainable lithium extraction from treated shale gas wastewater.

Keywords: Lithium recycling; $H_{1.33}Mn_{1.67}O_4$; Al doping; Shale Gas Wastewater (SGW); Adsorbent particles; Reverse osmosis concentrated water (ROC)

1. Introduction

Lithium is highly valued for its exceptional physical and electrochemical properties, as well as its broad applications in fields such as transportation, aerospace, chemistry, medicine, and energy—particularly in energy storage batteries [1-3]. Current lithium recycling efforts primarily target saline lakes and battery wastewater, while lithium resources in shale gas wastewater (SGW) have remained comparatively underexplored [4]. In the Sichuan Basin, the median lithium concentration in SGW is approximately 33 mg/L [5, 6]. By 2030, China is projected to produce 100–150 million m^3 of SGW, which, at this concentration, would contain 17,564–26,346 tons of lithium carbonate equivalent. However, the low lithium concentration in SGW poses challenges for its recovery [7].

A combined process including reverse osmosis (RO) membrane technology is currently the most practical and widely used method for treating SGW [8]. The RO process generates a substantial amount of reverse osmosis concentrate (SGW-ROC), characterized by higher salinity and further enriched lithium ions, making it a more viable resource for lithium recovery than the more diluted feed solution [9, 10]. However, reverse osmosis concentrate also contains a significant amount of organic matter, which can adversely affect the performance of lithium adsorbents. To address this issue, combination of biological treatment and adsorption on activated carbon has been proposed [9, 11].

Currently, techniques for concentrating or extracting lithium from aqueous solutions include lithium salt precipitation via evaporation[12], solvent extraction [13],

adsorption by adsorbents [14], nanofiltration and reverse osmosis [15], electrochemical techniques [16], or a combination of such techniques. Among these, manganese-based adsorbents are particularly advantageous due to their excellent adsorption capacity, selectivity, regeneration behavior, and low cost [17]. Within this category, $H_{1.33}Mn_{1.67}O_4$ is simpler to synthesize than alternatives, such as $H_{1.6}Mn_{1.6}O_4$ [18] or HMn_2O_4 [19], owing to the lower energy requirements of the preparation methods [20]. In our previous work, we synthesized aluminum-modified manganese-based adsorbents, which enhanced the performance of unmodified adsorbents by over 50% [21]. However, the inherent cohesiveness of the powder resulted in poor flowability, difficulties in fluidization, and substantial material loss during filtration [22]. In fact, the challenges associated with powder-based adsorbents limit their practical application. One effective solution is to aggregate the powder into monolithic structures, which can be achieved with techniques such as powder granulation, film immobilization, plastic foaming, and nanoscale fiber fabrication. Of these methods, granulation is the simplest and most cost-effective technique for various industrial applications [23].

Ryu et al. [24] synthesized manganese-based powder particles using petroleum-based asphalt as a binder, achieving an adsorption capacity of only 10 mg/g. Lai et al. [25] employed epoxy resin as a bonding agent to form manganese-based powder into adsorbents, which increased the adsorption capacity to 16 mg/g. Ryu et al. [26] and Hong et al. [27] further developed manganese-based powder into particle pellets using adhesives to produce adsorbent particles. Li et al. [21] and Zhang et al. [28] synthesized spherical particles using polyvinyl chloride (PVC) as a binder and a lithium-ion sieve

precursor. PVC is an inexpensive material that offers excellent mechanical properties, resistance to acids and alkalis, and ease of manufacture [29]. However, despite its advantages, PVC-based adsorbents are generally characterized by lower lithium adsorption capacities compared to powdered adsorbents [30], primarily due to the hydrophobic nature of PVC, which impedes lithium ion diffusion into the adsorbent matrix. To address this, The hydrophilic modifiers, such as polyacrylonitrile (PAN) [31], chitosan [32], or polyacrylamide (PAM) [33] have been introduced. Among various modifiers, CA and F127 have distinct advantages: CA contributes a surface layer rich in hydroxyl groups, imparting hydrophilicity, while the poly(ethylene oxide) (PEO) segments in F127 form micellar structures that improve water compatibility within the PVC matrix. Both modifiers are non-toxic and widely used in hydrophilic membrane fabrication. For example, Zhang et al. [34] incorporated CA into PVC to enhance hydrophilicity and reduce membrane fouling. Ahmad et al. [35] fabricated ultrafiltration membranes with F127 and PVC to reduce the contact angle of the membrane below 10° and to increase the permeate flux of the membrane. However, if the proportion of hydrophilic modifier in the final material is too high, this may lead to a brittle structure.

In this study, we present the fabrication of hydrophilically modified, aluminum-doped manganese-based adsorbent particles (HAMO-X; X = 1, 2, 3) via an anti-solvent phase transformation method. We first discuss the synthesis approach, which consists of blending the precursor powder with poly(vinyl chloride) (PVC) as a binder and either cellulose acetate (CA) or Pluronic F-127 (F127) as a hydrophilic modifier. We then provide information on the materials characteristics and their adsorption performance

when applied on reverse osmosis (RO)-concentrated water from a shale gas wastewater treatment facility in Sichuan, chosen for its relatively high lithium (Li) content. Next, we examine the adsorption kinetics and isotherms, and we present the performance of fixed-bed experiments with the most effective CA-modified particles. Finally, we assess the adsorbent reusability through cycling experiments. Our findings demonstrate that hydrophilic modification enhances material cost-effectiveness and lithium recovery from SGW, supporting the practical deployment of manganese-based adsorbents for industrial lithium extraction.

2. Materials and methods

2.1. Water source and materials

The reverse osmosis concentrate used in the experiment was the effluent of activated carbon BAF treatment at a shale gas treatment facility in Changning, Sichuan Basin, China [9]. The physical parameters of the shale gas wastewater constituents are summarized in **Table S1** of the Supporting Information (SI). $MnCO_3$, Li_2CO_3, and HCl of analytical grade were purchased from Sichuan Kelong Chemical Reagent Company, China. Cellulose acetate (CA) with 39.8 wt.% acetyl and 3.5 wt.% hydroxyl was obtained from Aladdin. Polyvinylpyrrolidone (PVP K30) and Pluronic F-127 (F127) were purchased from Sigma-Aldrich. Polyvinyl chloride (PVC) and dimethylacetamide (DMAC) were supplied by McLean Biochemicals Ltd.

2.2. Preparation of $Li_{1.33}Al_XMn_{1.67-X}O_4$ (LAMO) powder

The preparation of $Li_{1.33}Mn_{1.67}O_4$ (LMO) modified with aluminum (Al) was performed using Li_2CO_3, $MnCO_3$, and $AlCl_3 \cdot 6H_2O$ in specific proportions. These materials were ground at 200 rpm for 30 minutes using a grinder and then calcined in a tube furnace at a controlled temperature to produce the $Li_{1.33}$ $Al_{0.08}Mn_{1.59}O_4$ (LAMO) precursor powder. We provide detailed manufacturing procedures in **Text 2 (SI)** and in a previous work [21].

2.3. Preparation of HAMO powder and granular HAMO-X (X=1,2,3)

The standard LAMO precursor powder was treated with 0.1 mol/L HCl for 2 hours to elute lithium ions (Li^+) and obtain the corresponding adsorbent powder, referred to as HAMO. Additionally, the precursor powder was processed into pellets using the antisolvent method. These pellets were formulated with a pore forming agent and PVC as a binding agent, with or without a hydrophilic modifier. To determine the optimal composition, preliminary tests were conducted to evaluate different dosages of the hydrophilic modifier and pore forming agent. Based on these tests, three adsorbents were synthesized for the experimental study: HAMO-1 (PVC and pore forming agent), HAMO-2 (PVC, pore forming agent, and cellulose acetate as a hydrophilic modifier), and HAMO-3 (PVC, pore forming agent, and F127 as a hydrophilic modifier). For illustrative purposes, the synthesis of HAMO-2 is described in detail. A mixture of 5.6 wt.% PVC and 1.4 wt.% cellulose acetate (CA) was dissolved in 80 wt.% N,N-dimethylacetamide (DMAC) in a three-neck flask. The solution was stirred in a water bath at 55 ℃ until fully dissolved. Subsequently, 0.7 wt.% pore forming agent (PVP-

K30) was added and stirred until completely dissolved. Next, 8 wt.% LAMO adsorbent powder was incorporated, and the mixture was stirred for 5–6 hours to ensure a homogeneous slurry. Spherical black particles (~2.5 mm in diameter) with embedded manganese-based adsorbent precursor powder were formed via precipitation using the antisolvent method, leveraging PVC's insolubility in the aqueous phase. The final granular adsorbent was then treated with 0.1 mol/L HCl for 2 hours to elute lithium ions (Li^+). The other two adsorbents, HAMO-1 and HAMO-3, were synthesized using an analogous process but with different initial component mixtures. Detailed information on the compositional ratios of HAMO-X (X = 1, 2, 3) (e.g., **Table S2**, **SI**), as well as other particle fabrication methods and particle properties, are provided in the Supplementary Information to this paper, including exploring the issue of optimal ratios of hydrophilic modifier CA and optimal pore forming agent dosage.

2.4. Analysis and testing methods

The cross-sectional morphology of the adsorbent particles and the uniformity of powder dispersion were examined using field emission scanning electron microscopy (FE-SEM, Hitachi, Japan). The elemental distribution of Mn and Al was determined with energy dispersive spectroscopy (EDS). The structural changes of the doped adsorbent powders after granulation and the structural crystallinity of the hydrophilic modifications were investigated using X-ray diffraction (XRD), with a Regaku instrument from Rigaku, Japan. The material composition of the particulate adsorbent was tested with Fourier transform infrared spectroscopy (Perkelmer, USA). To

characterize surface properties and porosity, nitrogen physisorption measurements at 77 K were conducted with an ASAP 2460 analyzer (Micromeritics, USA) operating under cryogenic conditions. This investigation yielded adsorption-desorption isotherms from which surface area parameters were derived through the Brunauer-Emmett-Teller (BET) theory applied to nitrogen desorption data. Pore architecture quantification was achieved using the Barrett-Joyner-Halenda (BJH) methodology to determine size distributions, volumetric pore capacity, and surface area contributions across mesoporous domains. Hydrophilic characteristics were assessed through sessile drop measurements recorded with a KRÜSS GmbH contact angle goniometer (Hamburg, Germany), with instantaneous water droplet profiles captured for analysis. The amount of organics in aqueous samples was determined through total organic carbon quantification with a TOC-L analyzer (Shimadzu, Japan). Concurrently, ionic speciation in aqueous matrices was determined through atomic absorption spectroscopy employing a PinAAcle 900 T spectrometer (PerkinElmer, USA) to quantify dissolved metal concentrations.

2.5. Adsorption performance experiment

To investigate the adsorption kinetics, 0.5 g of wet composite particle adsorbent was weighed and mixed with 50 mL of SGW-ROC in a conical flask. The flask was placed in an oscillating incubator set at 25 ℃ and operated at 150 rpm for oscillatory adsorption. Samples of the supernatant were collected at various time intervals (t = 1, 3, 6, 9, 12, 24, 36, 48 hours), and the corresponding adsorption capacities were

calculated using the following equation.

$$q_t = \frac{(C_0 - C_t)V}{m} \quad (1)$$

Where, q_t (mg/g) represents the adsorption capacity of the composite particles at time t, C_0 (mg/L) represents the original concentration of Li^+ in the initial wastewater, C_t (mg/L) represents the concentration of Li^+ in the adsorbed liquid at time t, m (g) represents the mass of the adsorbent, and V (L) represents the amount of adsorbed liquid used by the adsorbent.

Lithium adsorption isotherms were also analyzed. Specifically, 0.05 g, 0.1 g, 0.2 g, 0.3 g, 0.4 g, and 0.5 g of composite adsorbent particles were added to 40 mL of SGW-ROC solution. The samples were placed in a shaking bed at 25 ℃ and agitated at 150 rpm for 48 h. The corresponding results were obtained in terms of lithium concentration in the liquid phase, and the necessary calculations were performed to determine the adsorbed amount at equilibrium, q_e (mg/g):

$$q_e = \frac{(C_0 - C_e)V}{m} \quad (2)$$

where, C_0 (mg/L) represents the original concentration of Li^+ in the initial wastewater, C_t (mg/L) represents the concentration of Li^+ in the liquid at equilibrium, m (g) represents the mass of adsorbent, and V (L) represents the amount of adsorbed liquid used by the adsorbent.

Upon lithium desorption with HCl, the concentrations of Mn^{2+}, Na^+, and K^+ in the solution were quantified using atomic absorption spectroscopy (AAS). The formulas for calculating Mn loss are provided in SI **Text S4**. In addition, to analyze the selectivity

of the adsorbent materials against different cations, the solutions were analyzed using atomic absorption spectroscopy (AAS), and the partition coefficients (K_d) were thus calculated. Additional parameters of this analysis are provided in SI **Text S8** and **Table S7**. Finally, to evaluate the impact of organic matter in SGW-ROC before and after adsorption, the dissolved organic carbon (DOC) content in water was analyzed using a TOC analyzer.

2.6. Fixed bed adsorption

The experimental setup for fixed bed adsorption tests is shown in **Fig. S2 (SI)**. Adsorption experiments were conducted using only the optimized adsorbent, 1.4-CA-0.7-PVPk30 (HAMO-2) and utilized a bottom-to-top liquid flow with continuous intake, handling 1 L or more of solution. Desorption was performed using 200 mL of 0.1 mol/L HCl acid over 220 minutes. A residence time of 40 minutes was used in the cyclic experiments, where adsorption involved 400 mL of SGW-ROC, followed by desorption with 15 mL of 0.1 mol/L HCl for 2 h. The specific pump speed value corresponding to EBCT is provided in **Table S3**.

3. Results and discussion

3.1 Structure and Chemical Properties of HAMO-X (X=1, 2, 3)

The representative XRD patterns of HAMO, HAMO-1, HAMO-2, and HAMO-3 are shown in **Fig. 1A**. The three major characteristic peaks of HAMO powder, located at approximately 19.05°, 36.95°, and 44.95°, correspond to the (111), (311), and (400) crystal planes within the spinel structure. The primary peaks of the composite HAMO-

X, at approximately 19.07°, 37.08°, and 45.1°, aligned with the (111), (311), and (400) planes, indicating successful incorporation of HAMO powder into the PVC matrix. The (111) peaks showed a slight increase relative to PVC, which can be attributed to the presence of organic substances, such as CA or F127. Furthermore, all characteristic peaks of the manganese crystal structure were retained, but their intensity significantly decreased, suggesting that the powder adsorbent and PVC were fully encapsulated and well-mixed. **Fig. 1B** indicates minor changes in the spinel peak positions for the CA-modified granular adsorbent material before (HAMO-2) and after its utilization for adsorption of lithium (r-LAMO-2). These changes are probably a result of the reciprocal exchange between Li^+ and H^+ ions, alongside variations in their ionic radii, which could lead to modifications in the dimensions of the crystalline cell [21].

Representative FTIR spectra of the three adsorbent particles are shown in **Fig. 1C**, along with the IR spectra of the optimal adsorbent in its various synthesis and use steps (**Fig. 1D**). According to the literature, the characteristic peaks of PVC include a variety of absorption bands. In the infrared spectrum, the vibrational band observed at 2911 cm^{-1} may be assigned to asymmetric stretching modes within methyl/methylene functional groups[36]. Further spectral analysis reveals features at 1422 cm^{-1} and 1250 cm^{-1}, which suggest symmetric deformation in methylene units and aliphatic C-C bond stretching, respectively[37]. The absorption peak at 957 cm^{-1} is attributed to a coupled lattice vibration of the proton [38]. The peak at 600 cm^{-1} is instead attributed to the C-Cl stretching vibration [39]. Therefore, the FTIR spectra of the three adsorbent particles, HAMO-X, showed the characteristic peaks of both PVC and HAMO, supporting the

successful incorporation of HAMO into the binding material. When examining the specific spectra of HAMO-2, LAMO-2, and r-LAMO-2, a distinct absorption peak appearing near 1750 cm^{-1}—assigned to the carbonyl C=O stretching of ester—suggests the fact that CA was successfully incorporated into the PVC material for this specific adsorbent [37]. The hydrophilic groups (-OH) of CA are retained or partially exposed on the material's surface, forming a hydroxyl-rich outer layer that promotes stronger interactions with water molecules, thereby enhancing the overall hydrophilicity of the material.

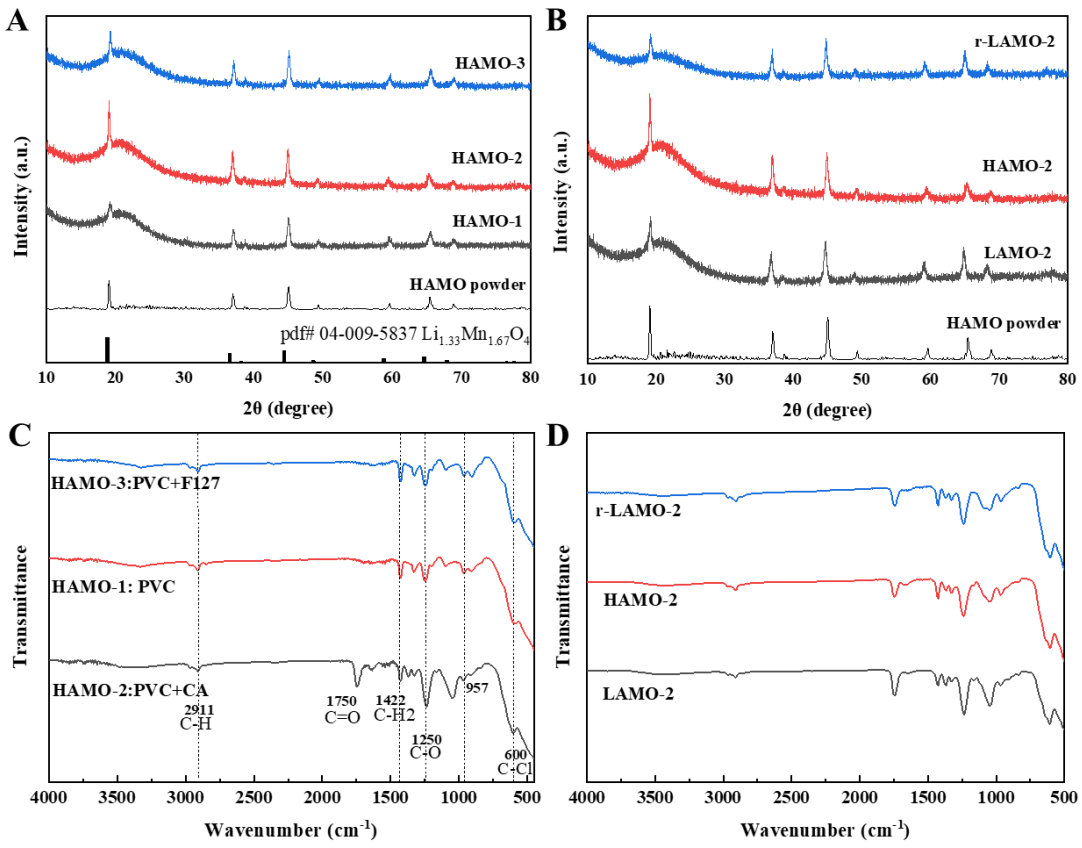

Fig. 1. (A) XRD patterns of HAMO-1, HAMO-2, and HAMO-3, as well as the standard powder HAMO and pdf# 04-009-5837 $Li_{1.33}Mn_{1.67}O_4$. (B) XRD pattern of the CA-modified adsorbent, in its various synthesis and use steps, namely, the adsorbent

277 precursor LAMO-2, the CA-modified adsorbent HAMO-2, and the adsorbent following
278 its utilization to adsorb lithium from SGW-ROC (r-LAMO-2), as well as the standard
279 powder HAMO. (C) FTIR spectra of HAMO-1, HAMO-2, and HAMO-3. (D) FTIR
280 spectra of the CA-modified adsorbent, in its various synthesis and use steps.
281
282 **Fig. 2A-F** show that the cross-sections of the three adsorbent particles exhibited a
283 spherical-like morphology, with loose and porous interiors and microporous structures
284 on the surface. This characteristic was particularly pronounced in particles modified
285 with CA and F127. **Fig. 2H-I** suggest that, at higher magnifications, particles modified
286 with CA achieved a more uniform dispersion of the HAMO powder within the particles.
287 This uniform distribution is expected to enhance the contact with lithium in the solution,
288 thereby improving the adsorption performance. Energy-dispersive spectroscopy (EDS)
289 surface scans in **Fig. 2J-Q** indicated that manganese (Mn) and aluminum (Al) were
290 uniformly distributed in all three adsorbent particles, suggesting effective doping of the
291 HAMO powder into the PVC skeleton. However, the uniformity of the CA-modified
292 particles was more pronounced. **Fig. S7 (SI)** indicates that, as the proportion of pore-
293 forming agent increased, the voids within the particles became progressively larger. The
294 cross-sectional morphology of the particles before and after their deployment in lithium
295 adsorption, as shown in **Fig. S8 (SI)**, indicated minimal changes, with materials
296 maintaining a uniform structure across their thickness.
297

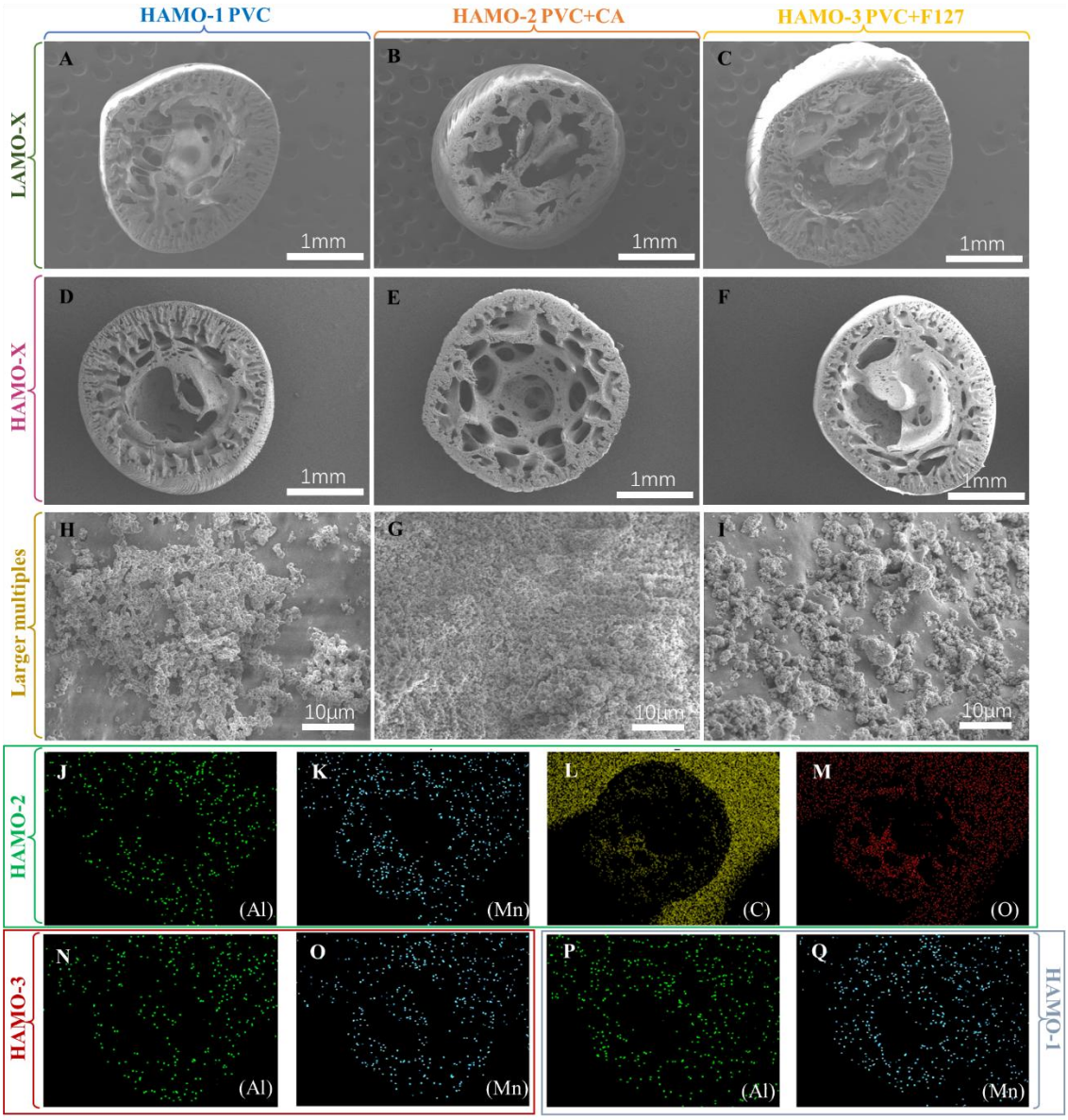

Fig. 2. Representative SEM micrographs: (A-C) Comparative results of three material cross sections, namely, PVC, PVC+CA, PVC+F127 for LAMO-X, and for HAMO-X (X=1,2,3). (H-I) Magnification of cross sections of HAMO-1, HAMO-2, and HAMO-3. Comparison of Al, Mn, C, and O elements (J-M) in the cross section of CA-modified adsorbent particles (HAMO-2); (N-O) F-127-modified particles (HAMO-3), and unmodified PVC particles (HAMO-1).

Fig. 3A presents the nitrogen adsorption-desorption isotherms of HAMO-1,

HAMO-2, and HAMO-3 composite particle adsorbents. All three adsorbents displayed the typical type IV isotherm and featured H3 hysteresis loops [40]. This performance closely resembled that of the HAMO powder, confirming the successful incorporation of HAMO powder into the particles. The nitrogen adsorption capacities of HAMO-1, HAMO-2, and HAMO-3 were 30.32, 39.64, and 21.22 cm^3/g (STP), respectively. The pore size distributions, derived from the desorption branch of the nitrogen adsorption-desorption isotherms using the BJH method, are displayed in **Fig. 3B**. **Fig. 3C** illustrates isothermal relative pressures ranging from 0.07 to 0.26, with higher values corresponding to smaller BET surface areas. The BET surface areas of HAMO-1, HAMO-2, and HAMO-3 were calculated as 11.32, 16.08, and 8.82 m^2/g, respectively. Among these, HAMO-2, that is, the adsorbent material with inclusion of CA into the HAMO/PVC matrix, demonstrated the highest nitrogen adsorption capacity and surface area. Contact angle measurements in **Fig. 3D-F** revealed significant differences in the hydrophilicity of the three adsorbents. Notably, the contact angle of HAMO-2 was 48°, indicating a higher affinity with water compared to the other materials.

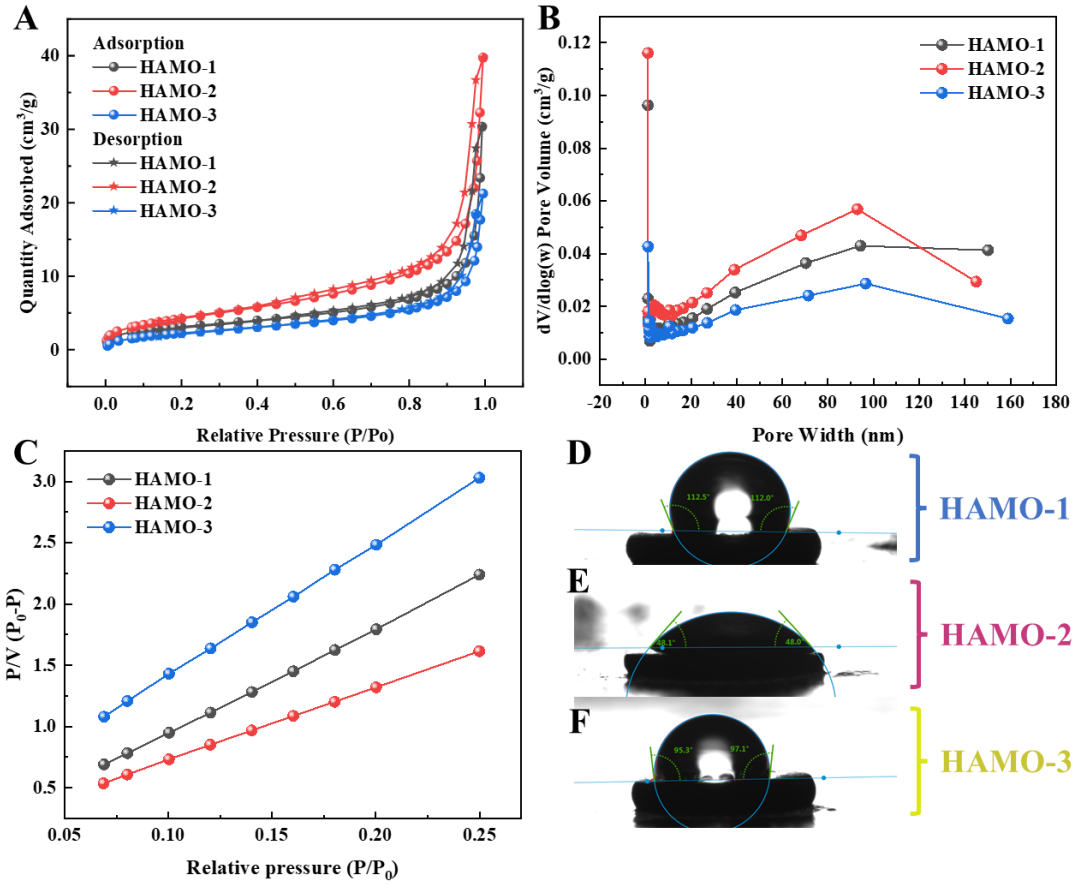

Fig. 3. (A) Nitrogen adsorption-desorption isotherm plots of the three composite particle adsorbents. (B) Pore size distribution. (C) BET specific surface area plot. (D-F) Representative images of water droplets used to evaluate contact angles.

3.2. Adsorption behavior and selectivity of HAMO-X

Equilibrium adsorption tests indicated that the Freundlich model provided a slightly better fit compared to the Langmuir model; see **Table 1** for fitting parameters and **Fig. 4D-E** for the raw data and fitting curves. The stronger correlation with the Freundlich isotherm model suggests the presence of compound adsorption layers on the adsorbent material surface [41, 42]. Under optimized conditions, the maximum lithium uptake capacity reached 28.7 mg/g at a dosage of 0.5 g of hydrated sorbent per 40 mL

of shale gas wastewater reverse osmosis concentrate. The Weber-Morris (W-M) internal diffusion model was also used to fit the data, with results shown in **Table S6** and **Fig. 4H**, demonstrating that the initial hours of the adsorption process were dominated by diffusion, followed by the onset of chemisorption until equilibrium.

The kinetic fitting results for the two adsorption models are presented in **Fig. 4A-B** and **Table 2**. Lithium adsorption by HAMO-X (X = 1, 2, 3) was most rapid within the first 10 hours before gradually leveling off as equilibrium was reached. For HAMO-2, the R^2 values exceeded 0.95, with 0.980 for the pseudo-first-order model and 0.990 for the pseudo-second-order model, indicating that both physical and chemical processes contributed to adsorption, with chemisorption likely being dominant. Physical adsorption occurred via attachment to the PVC matrix, while chemisorption was driven by electron valence forces associated with ion exchange. The R^2 values obtained with the Elovich model (**Table S5**), which was slightly lower than the pseudo-secondary kinetics but substantially higher than the pseudo-primary model, further supports the conclusion that the adsorption process was dominated by chemisorption and that the energy distribution of the surface sites was uneven.

Notably, PVC particles modified with CA achieved a higher adsorption capacity of approximately 20.2 mg/g, slightly exceeding the capacities of both unmodified PVC particles and those modified with F127. This improved performance may be attributed to the hydrophilic modification introduced by CA, which facilitated better contact between Li^+ in water and the manganese-based adsorbent particles, enhancing lithium recovery from SGW-ROC containing organic matter.

Table 1 Fitting Parameters from Adsorption Isotherm Models

	Adsorption isotherms					
	Langmuir model			Freundlich model		
	Q_m (mg/g)	K_L (L/mg)	R^2	K_F ($mg^{1-1/n} \cdot L^{1/n}/g$)	n ($g \cdot mg^{-1}L^{-1}$)	R^2
HAMO-1	27.4	0.049	0.870	12.84	5.22	0.963
HAMO-2	28.7	0.112	0.858	13.81	5.27	0.984
HAMO-3	27.7	0.801	0.878	11.32	4.49	0.968

Table 2 Parameters from Data Fitting with Kinetics Models

	Adsorption kinetics					
	Pseudo-first-model			Pseudo-second-model		
	$q_{e,cal}$ (mg/g)	k_1 (h^{-1})	R^2	$q_{e,cal}$ (mg/g)	k_2 ($g \cdot mg^{-1}h^{-1}$)	R^2
HAMO-1	16.7	0.200	0.975	18.8	0.0143	0.993
HAMO-2	18.4	0.256	0.980	20.2	0.0187	0.990
HAMO-3	16.3	0.278	0.958	18.0	0.0223	0.983

In industrial applications, SGW undergoes various treatment processes that decrease the concentrations of Ca^{2+} and Mg^{2+} before entering the reverse osmosis system, partially reducing the competition of other cations for Li adsorption and making SGW-ROC a more viable resource for lithium recovery. Additionally, the RO process generates a concentrate stream with high salinity and enriched lithium ions, which accelerates Li adsorption kinetics and improves the process's economic feasibility. However, the RO brine still contains high concentrations of competing ions, particularly Na^+ and K^+, which can impact selectivity. The lithium selective separation performance of the three particulate adsorbents tested in concentrated shale gas wastewater treatment is presented in **Fig. 4G**. The extraction separation coefficients for Li^+ were 3207 mL/g, 4479 mL/g, and 3950 mL/g for HAMO-1, HAMO-2, and HAMO-

3, respectively. These results demonstrate that hydrophilic modifications significantly improved lithium selectivity, with cellulose acetate proving to be the most effective modifier. The corresponding adsorption selectivity parameters are provided in **Table S7** of the **SI**. The specific adsorption capacity of the CA-modified hydrophilic adsorbent is illustrated in **Fig. 4I** and **Table S5 (SI)**, highlighting its superior performance compared to many previously reported adsorbents.

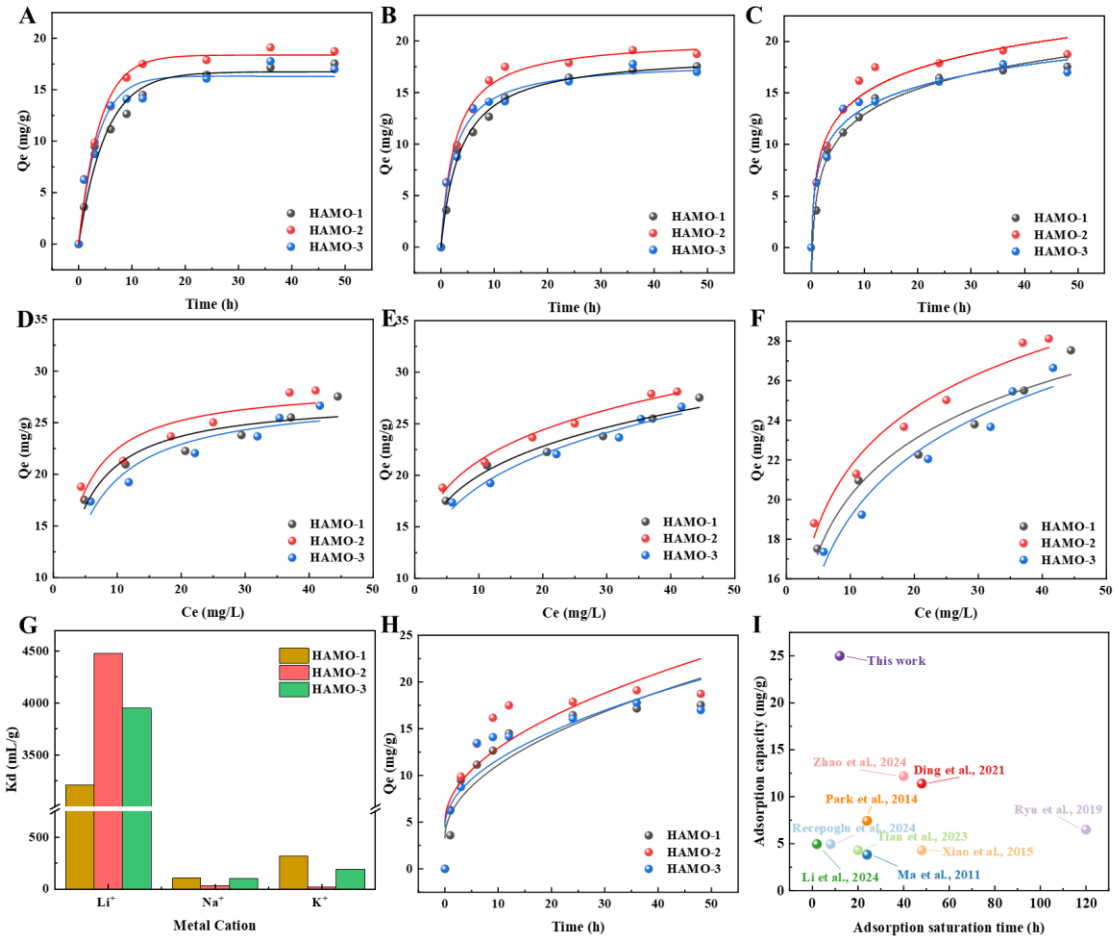

Fig. 4. Adsorption data and modeling. SGW lithium adsorption kinetics data fitted with (A) pseudo-first-order kinetics. (B) pseudo-second-order kinetics. (C) Elovich kinetics. SGW lithium equilibrium adsorption data fitted with (D) Langmuir, (E) Freundlich, and (F) Temkin equilibrium models. (G) Adsorption selectivity of HAMO-2 adsorbent. (H)

Adsorption kinetics data fitted with the Weber-Morris (W-M) internal diffusion model.

(I) Comparative adsorption capacity performance of adsorbents from the literature.

3.3. Fixed bed adsorption

Based on the results discussed above, HAMO-2 was selected as the most promising material for lithium adsorption and was thus utilized to produce a fixed bed for depth filtration of the SGW-ROC stream and assess lithium adsorption, material stability, and Mn loss.

3.3.1 Optimization of parameters: EBCT and HCl concentration for lithium recovery

Empty bed contact time (EBCT) represents the duration for which water flows through a treatment unit and remains in contact with various types of beds. Minimizing EBCT is desirable for process efficiency; however, excessively short EBCT may reduce lithium extraction efficiency if the solution flow rate through the granular bed surpasses the timescales of adsorption [23, 43]. Therefore, the effect of different EBCT values on adsorption capacity and bed volume in fixed-bed tests was evaluated. **Fig. 5A** and **Fig. 5B** illustrate the lithium recovery performance using CA-modified PVC composite particle adsorbents in SGW-ROC. The breakthrough times ($C/C_0 = 0.9$) were 8.5 h, 28.7 h, 34.9 h, and 37.5 h for EBCT values equal to 15, 30, 40, and 60 minutes, respectively. The corresponding adsorption capacities at the breakthrough point were 1.6 mg/g, 2.3 mg/g, 12.6 mg/g, and 8.8 mg/g. Therefore, an EBCT of 40 minutes resulted in an adsorbed liquid volume exceeding 40 times the empty bed volume, highlighting the remarkable adsorption performance of HAMO-2 under these conditions. These results

indicate that higher flow rates (i.e., EBCT values shorter than 40 min) led to insufficient residence time in the column and inadequate mass transfer mechanisms [44]. However, an excessively long residence time may enhance the influence of organic matter on lithium adsorption **(Fig. S13).** As shown in **Fig. 5B**, the lithium concentration in the initial effluent during cyclic desorption experiments was high after treatment with the acid solution, regardless of the desorption flow rate. However, it quickly stabilized at approximately 175 mg/L. These results indicate that precise control of desorption time could yield a solution with a high lithium concentration.

Manganese-based adsorbents experience elemental Mn loss during desorption due to disproportionation of the Mn valence state, triggered by the reaction between Mn and the acidic solution used for lithium extraction upon bed utilization for adsorption. Consequently, the extent of Mn loss serves as a critical indicator of the adsorbent's operational performance [45]. **Fig. 5D** and **5F** present the results of Mn loss during fixed-bed cyclic experiments using different concentrations of HCl in acid leaching tests. When 0.1 mol/L HCl was used, manganese loss was controlled to less than 0.3%, a substantially lower value compared to the use of more concentrated acid solution. At the same time, 0.1 mol/L HCl provided a lithium concentration in the desorbed solution of approximately 500 mg/L, which was only slight lower than that achieved using more acidic solutions. These results suggest that an optimization considering both Mn loss and lithium recovery may be achieved, with 0.1 mol/L HCl providing an optimal balance between these phenomena. For all the tests described above, a EBCT of 40 min was used, together with an HCl concentration equal to 0.1 mol/L.

3.3.2. Stability of the adsorbent material and interaction with organic matter

Since shale gas wastewater typically contains substantial amounts of organic matter, understanding its effect on adsorbent particles is essential. **Fig. 5G** and **5H** demonstrate that CA-modified particles exhibited suitable adsorption performance at an organic matter concentration of 51.3 mg/L. In the fixed bed effluent, the organic matter concentration was comparable to that of the raw water across various time periods, suggesting that CA-modified PVC had a negligible effect on organic matter adsorption in the raw water. Furthermore, the mass concentrations of organic matter in the rinsing and desorbing solutions were 12.7 mg/L and 20.3 mg/L, respectively, confirming that the organic matter adsorbed by the particles can be effectively desorbed through water washing and acid treatment.

The stability adsorption of HAMO-2 particles was tested over 10 cycles, with the specific cycle shown in **Fig. 5I** as an example. After 10 cycles, the solution remained clear and transparent, the particles remained intact, and the adsorption capacity showed no substantial change. The manganese (Mn) loss from the Al-modified Mn-based material was 0.45% after the first cycle, decreasing to approximately 0.3% and eventually dropping to below 0.2% in subsequent desorption cycles. The higher manganese loss observed during the initial cycle is attributed to the incomplete immobilization of manganese within the PVC matrix during the granulation process. Consequently, Mn on the surface of the crystals was easily eluted when exposed to the desorption solution, resulting in a higher Mn loss at the start of the process, followed

by stabilization at a lower rate [46]. Overall, the stability of CA-modified particles suggests their potential for long-term applications in lithium recovery.

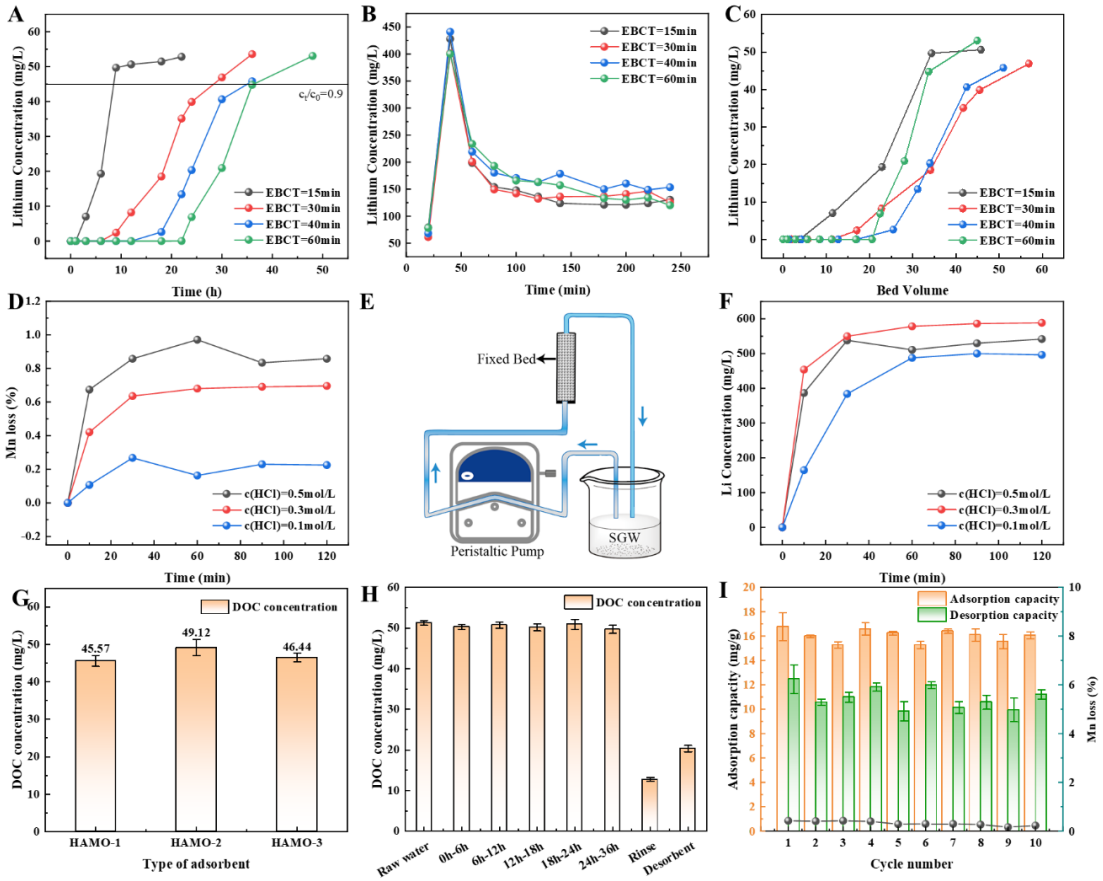

Fig. 5. (A) Concentration of Li in the effluent from the fixed adsorption bed vs. time. (B) Results of Li desorption using hydrochloric acid at different residence times. (C) Relationship between the inlet volume of fixed bed and Li concentration in the effluent; (D) Study of the Mn concentration loss in HCl at different concentrations; (E) Schematic diagram of the fixed bed in the cycling experiment; (F) Concentration of Li in the desorbing solution using HCl at different concentrations; (G) Concentration of organic matter remaining in solution after adsorption starting from a concentration of 51.3 mg/L in the SGW-ROC. (H) Residual concentration of TOC in the fixed-bed effluent at different times of adsorption and phases of the cycle. (I) Adsorption capacity

462 and Mn loss in the various cycles of the cyclic experiment.

463

464 **4. Conclusion**

465 This study synthesized and characterized aluminum-modified manganese-based
466 ion sieves ($H_{1.33}Al_{0.08}Mn_{1.59}O_4$, referred to as "HAMO") in the form of composite
467 particles by incorporating polyvinyl chloride (PVC) and introducing hydrophilic
468 modifications using cellulose acetate (CA), Pluronic F-127 (F127), and/or
469 polyvinylpyrrolidone K30 (PVP-K30). Among the tested modifications, CA-modified
470 adsorbent particles demonstrated a loose and porous structure with a uniform internal
471 distribution of manganese-based powder, enhanced hydrophilicity, and minimal
472 morphological changes before and after lithium adsorption. The CA-modified PVC
473 particles (designated as HAMO-2) exhibited superior lithium adsorption capacity (20.2
474 mg/g) and lithium/particle partition coefficient (4.48 mL/g) compared to F127-
475 modified counterparts. This performance is attributed to increased surface polarity,
476 larger specific surface area, and improved chemisorption properties. Notably, the
477 adsorption capacity of HAMO-2 exceeded 25 mg/g when applied to SGW-ROC at an
478 adsorbent dosage of 0.1 g/40 mL. Even after 10 adsorption-desorption cycles under
479 optimal fixed-bed empty-bed contact time (EBCT) of 40 minutes, the material
480 maintained both structural integrity and stable adsorption performance, with manganese
481 loss limited to approximately 0.3%. Future work will aim to further optimize the
482 relationship between particle modification and adsorption performance, reduce
483 manganese leaching, and enhance operational efficiency to broaden potential

application scenarios.

Acknowledgments

This work was supported by the National Natural Science Foundation of China (52070134, 52270075), Leading Scientific and Technological Talents Cultivation Program (2023SCU17), the Sichuan University and Zigong City People's Government Strategic Cooperation Project (2022CDZG-7), the Outstanding Youth Science Foundation of Sichuan Province Natural Science Foundation (2025NSFJQ0010), and Dongfang Electric Corporation (Dongfang Boiler) University-Enterprise Cooperation Project (24H0846). A.T. acknowledges the support of Politecnico di Torino. The views and ideas expressed herein are solely those of the authors and do not represent the ideas of the funding agencies in any form.

References

[1] B. Swain, Recovery and recycling of lithium: A review, Sep. Purif. Technol., 172 (2017) 388-403. https://doi.org/10.1016/j.seppur.2016.08.031

[2] A. Battistel, M.S. Palagonia, D. Brogioli, F. La Mantia, R. Trócoli, Electrochemical Methods for Lithium Recovery: A Comprehensive and Critical Review, Adv. Mater., 32 (2020). https://doi.org/10.1002/adma.201905440

[3] Z. Sun, H. Cao, Y. Xiao, J. Sietsma, W. Jin, H. Agterhuis, Y. Yang, Toward Sustainability for Recovery of Critical Metals from Electronic Waste: The Hydrochemistry Processes, ACS Sustain. Chem. Eng., 5 (2017) 21-40. https://doi.org/10.1021/acssuschemeng.6b00841

[4] J. Hou, H.C. Zhang, A.W. Thornton, A.J. Hill, H.T. Wang, K. Konstas, Lithium Extraction by Emerging Metal-Organic Framework-Based Membranes, Adv. Funct. Mater., 31 (2021). https://doi.org/10.1002/adfm.202105991

[5] W.C. Xie, P. Tang, Q.D. Wu, C. Chen, Z.Y. Song, T. Li, Y.H. Bai, S.H. Lin, A. Tiraferri, B.C. Liu, Solar-driven desalination and resource recovery of shale gas wastewater by on-site interfacial evaporation, Chem. Eng. J., 428 (2022). https://doi.org/10.1016/j.cej.2021.132624

[6] L.O. Haluszczak, A.W. Rose, L.R. Kump, Geochemical evaluation of flowback brine from Marcellus gas wells in Pennsylvania, USA, Appl. Geochem., 28 (2013) 55-61. https://doi.org/10.1016/j.apgeochem.2012.10.002

[7] S.C. Mo, N. Sun, X.T. Liu, W.M. Zhu, T. He, Forward osmosis for concentrating lithium-enriched brine: From membrane performance to system design, Desalination, 591 (2024) 117997-118012. https://doi.org/10.1016/j.desal.2024.117997

[8] M. Yaqub, M.N. Nguyen, W. Lee, Treating reverse osmosis concentrate to address scaling and fouling problems in zero-liquid discharge systems: A scientometric review of global trends, Sci. Total Environ., 844 (2022) 157081-157100. https://doi.org/10.1016/j.scitotenv.2022.157081

[9] M.T. Zhu, P. Tang, X.L. Yu, F.M. Li, S.L. Shi, D. Zhang, J.L. Shi, W. Tao, X. Ruan, L.J. Liu, B.C. Liu, Effective and mechanistic insights into shale gas wastewater reverse osmosis concentrate treatment using ozonation-biological activated carbon process, Sci. Total Environ., 945 (2024) 174080-174088. https://doi.org/10.1016/j.scitotenv.2024.174080

[10] Z.L. Li, Y.J. Zhao, Y. Li, J.J. Lu, M. Wang, Reverse osmosis process combining energy consumption analysis and mass transfer in the concentration of lithium-enriched brine, Desalination, 594 (2025) 118309-118324. https://doi.org/10.1016/j.desal.2024.118309

[11] Y. Jang, E. Chung, Influence of Alkanes on Lithium Adsorption and Desorption of a H2TiO3 Ion Sieve Adsorbent in Synthetic Shale Gas-Produced Water, Ind. Eng. Chem. Res., 58 (2019) 21897-21903. https://doi.org/10.1021/acs.iecr.9b04472

[12] Y.F. Ma, S.Y. Huang, X. Liu, J. Huang, Y.M. Zhang, K.S. Li, Z.H. Zhang, X.S. Yu, Z.H. Fu, Lithium enrichment and migration mechanism in the evaporation process of sodium aulphate subtype salt lake brine, Desalination, 566 (2023). https://doi.org/10.1016/j.desal.2023.116908

[13] R. Coterillo, L.E. Gallart, E. Fernandez-Escalante, J. Junquera, P. Garcia-Fernandez, I. Ortiz, R. Ibanez, M.F. San-Roman, Selective extraction of lithium from seawater desalination concentrates: Study of thermodynamic and equilibrium properties using Density Functional Theory (DFT), Desalination, 532 (2022). https://doi.org/10.1016/j.desal.2022.115704

[14] J.W. Xu, X.Y. Wei, J.W. Han, W.Q. Qin, Synthesis and optimisation mechanism of functionalised adsorption materials for lithium-ion extraction from salt water: A review, Sep. Purif. Technol., 339 (2024) 126237-126259. https://doi.org/10.1016/j.seppur.2023.126237

[15] L. Wang, D. Rehman, P.F. Sun, A. Deshmukh, C.Y. Tang, Novel Positively Charged Metal-Coordinated Nanofiltration Membrane for Lithium Recovery, ACS Appl. Mater. Interfaces, (2021). https://doi.org/10.1021/acsami.1c02252
[16] L. Wu, C.Y. Zhang, S. Kim, T.A. Hatton, H.L. Mo, T.D. Waite, Lithium recovery using electrochemical technologies: Advances and challenges, Water Res., 221 (2022). https://doi.org/10.1016/j.watres.2022.118822
[17] R. Chitrakar, Y. Makita, K. Ooi, A. Sonoda, Selective Uptake of Lithium Ion from Brine by HMnO and HMnO, Chemistry Letters, 41 (2012) 1647-1649. https://doi.org/10.1246/cl.2012.1647
[18] L. Wang, J. Wang, X.D. Wang, Synthesis of zirconium-coated lithium ion sieve with enhanced cycle stability, Sep. Purif. Technol., 303 (2022) 121933-121944. https://doi.org/10.1016/j.seppur.2022.121933
[19] L.Y. Song, M.X. Liu, M. Nian, G. Yang, Preparation of HMnO lithium-ion sieves with low manganese dissolution loss for improved cycling stability, Rsc Advances, 14 (2024) 19795-19805. https://doi.org/10.1039/d4ra02757d
[20] L. Tian, Y.H. Liu, P. Tang, Y.S. Yang, X.R. Wang, T.X. Chen, Y.H. Bai, A. Tiraferri, B.C. Liu, Lithium extraction from shale gas flowback and produced water using H1.33Mn1.67O4 adsorbent, Resour. Conserv. Recy., 185 (2022) 106476-106485. https://doi.org/10.1016/j.resconrec.2022.106476
[21] X. Li, X. Li, G. Chen, D. Zhang, L. Tian, J. Chen, C. Liu, B. Li, A. Tiraferri, B. Liu, Efficient recovery of lithium from shale gas wastewater: Fe, Ni, and Al doping of $H_{1.33}Mn_{1.67}O_4$ for improved adsorption capacity and manganese loss reduction, J. Clean. Prod., 473 (2024) 143554-143563. https://doi.org/10.1016/j.jclepro.2024.143554
[22] X. Xu, Y.M. Chen, P.Y. Wan, K. Gasem, K.Y. Wang, T. He, H. Adidharma, M.H. Fan, Extraction of lithium with functionalized lithium ion-sieves, Prog. Mater Sci., 84 (2016) 276-313. https://doi.org/10.1016/j.pmatsci.2016.09.004
[23] L. Tian, Y. Yang, G. Chen, A. Tiraferri, B. Liu, Efficient Lithium Extraction from Shale Gas Wastewater Using Sodium Alginate/$H_{1.33}Mn_{1.67}O_4$ Composite Granular Adsorbents, ACS EST Engg., 3 (2023) 1676-1685. https://doi.org/10.1021/acsestengg.3c00167
[24] J.C. Ryu, J. Shin, C. Lim, K.H. Kim, T. Ryu, Y.S. Lee, Lithium ion adsorption characteristics of porous $Li_{1.33}Mn_{1.67}O_4$ adsorbent prepared using petroleum-based pitch as a binder, Hydrometallurgy, 209 (2022). https://doi.org/10.1016/j.hydromet.2022.105837
[25] X.R. Lai, Y.J. Yuan, Z.Q. Chen, J.H. Peng, H. Sun, H. Zhong, Adsorption-Desorption Properties of Granular EP/HMO Composite and Its Application in Lithium Recovery from Brine, Ind. Eng. Chem. Res., 59 (2020) 7913-7925. https://doi.org/10.1021/acs.iecr.0c00668
[26] T. Ryu, Y. Haldorai, A. Rengaraj, J. Shin, H.J. Hong, G.W. Lee, Y.K. Han, Y.S. Huh, K.S. Chung, Recovery of Lithium Ions from Seawater Using a Continuous Flow Adsorption Column Packed with Granulated Chitosan Lithium Manganese Oxide, Ind. Eng. Chem. Res., 55 (2016) 7218-7225. https://doi.org/10.1021/acs.iecr.6b01632
[27] H.J. Hong, I.S. Park, T. Ryu, J. Ryu, B.G. Kim, K.S. Chung, Granulation of $Li_{1.33}Mn_{1.67}O_4$ (LMO) through the use of cross-linked chitosan for the effective recovery of Li^+ from seawater, Chem. Eng. J., 234 (2013) 16-22. https://doi.org/10.1016/j.cej.2013.08.060
[28] G.T. Zhang, C.X. Hai, Y. Zhou, J.Z. Zhang, Y.H. Liu, J.B. Zeng, Y. Shen, X. Li, Y.X. Sun, Z.W. Wu, W.P. Tang, Synthesis and performance estimation of a granulated PVC/PAN-lithium ion-sieve for Li plus recovery from brine, Sep. Purif. Technol., 305 (2023) 122431-122442. https://doi.org/10.1016/j.seppur.2022.122431

[29] G. Xiao, K. Tong, L. Zhou, J. Xiao, J. Yu, Adsorption and Desorption Behavior of Lithium Ion in Spherical PVC–MnO_2 Ion Sieve, Ind. Eng. Chem. Res., 51 (2012) 10921–10929. https://doi.org/10.1021/ie300087s
[30] T. Ryu, D.H. Lee, J.C. Ryu, J. Shin, K.S. Chung, Y.H. Kim, A lithium selective adsorption composite by coating adsorbent on PVC plate using epoxy-silica hybrid binder, Hydrometallurgy, 183 (2019) 118-124. https://doi.org/10.1016/j.hydromet.2018.11.011
[31] A. Umeno, Y. Miyai, N. Takagi, R. Chitrakar, K. Sakane, K. Ooi, Preparation and adsorptive properties of membrane-type adsorbents for lithium recovery from seawater, Ind. Eng. Chem. Res., 41 (2002) 4281-4287. https://doi.org/10.1021/ie010847j
[32] H.J. Hong, I.S. Park, T. Ryu, J. Ryu, B.G. Kim, K.S. Chung, Granulation of $Li_{1.33}Mn_{1.67}O_4$ (LMO) through the use of cross-linked chitosan for the effective recovery of Li from seawater, Chem. Eng. J., 234 (2013) 16-22. https://doi.org/10.1016/j.cej.2013.08.060
[33] J.L. Xiao, S.Y. Sun, X.F. Song, P. Li, J.G. Yu, Lithium ion recovery from brine using granulated polyacrylamide-MnO ion-sieve, Chem. Eng. J., 279 (2015) 659-666. https://doi.org/10.1016/j.cej.2015.05.075
[34] Y. Zhang, L. Tan, A.R. Yao, P.F. Tan, R.H. Guo, M. Zhou, P.X. Zhu, S.J. Huang, Y.H. Wu, Improvement of filtration performance of polyvinyl chloride/cellulose acetate blend membrane via acid hydrolysis, J. Appl. Polym. Sci., 138 (2021). https://doi.org/10.1002/app.50312
[35] T. Ahmad, C. Guria, A. Mandal, Optimal synthesis, characterization and antifouling performance of Pluronic F127/bentonite-based super-hydrophilic polyvinyl chloride ultrafiltration membrane for enhanced oilfield produced water treatment, Journal of Industrial and Engineering Chemistry, 90 (2020) 58-75. https://doi.org/10.1016/j.jiec.2020.06.023
[36] R.N. Clark, J.M. Curchin, T.M. Hoefen, G.A. Swayze, Reflectance spectroscopy of organic compounds: 1. Alkanes, J Geophys Res-Planet, 114 (2009). https://doi.org/10.1029/2008je003150
[37] P.J. Linstrom, W.G. Mallard, The NIST Chemistry WebBook: A Chemical Data Resource on the Internet, Journal of Chemical & Engineering Data, 46 (2001) 1059-1063. https://doi.org/10.1021/je000236i
[38] L. Wang, L. Wang, L.P. Li, Preparation of PVC-LMZO membrane and its lithium adsorption performance from brine, Desalination, 561 (2023) 116689-116705. https://doi.org/10.1016/j.desal.2023.116689
[39] W. Qu, Y.C. Fu, Y.S. Zhang, W.C. Wang, C. Xu, C. Liu, Y. Zhang, Q. Wang, B.C. Liu, Structural/surficial dual regulated granular HTiO lithium-ion sieves for lithium extraction from salt lake brine, J. Clean. Prod., 449 (2024) 141789. https://doi.org/10.1016/j.jclepro.2024.141789
[40] M. Thommes, K. Kaneko, A.V. Neimark, J.P. Olivier, F. Rodriguez-Reinoso, J. Rouquerol, K.S.W. Sing, Physisorption of gases, with special reference to the evaluation of surface area and pore size distribution (IUPAC Technical Report), Pure Appl. Chem., 87 (2015) 1051-1069. https://doi.org/10.1515/pac-2014-1117
[41] J. Zhong, S. Lin, J.G. Yu, Li^+ adsorption performance and mechanism using lithium/aluminum layered double hydroxides in low grade brines, Desalination, 505 (2021) 114983-114993. https://doi.org/10.1016/j.desal.2021.114983
[42] Y.S. Ho, G. McKay, Pseudo-second order model for sorption processes, Process Biochem., 34 (1999) 451-465. https://doi.org/10.1016/S0032-9592(98)00112-5
[43] V.C. Srivastava, B. Prasad, I.M. Mishra, I.D. Mall, M.M. Swamy, Prediction of Breakthrough Curves for Sorptive Removal of Phenol by Bagasse Fly Ash Packed Bed, Ind. Eng. Chem. Res., 47

(2008) 1603-1613. https://doi.org/10.1021/ie0708475
[44] A. Goshadrou, A. Moheb, Continuous fixed bed adsorption of C.I. Acid Blue 92 by exfoliated graphite: An experimental and modeling study, Desalination, 269 (2011) 170-176. https://doi.org/10.1016/j.desal.2010.10.058
[45] A.L. Gao, Z.H. Sun, S.P. Li, X.J. Hou, H.Q. Li, Q.S. Wu, X.G. Xi, The mechanism of manganese dissolution on $Li_{1.6}Mn_{1.6}O_4$ ion sieves with HCl, Dalton Trans., 47 (2018) 3864-3871. https://doi.org/10.1039/c8dt00033f
[46] H. Li, J. Qin, K. Zhao, Y. Guo, B. Tong, M. Samadiy, U. Alimov, T. Deng, Novel lithium ion-sieve spinning fiber composite of PVDF-HMO for lithium recovery from geothermal water, J. Clean. Prod., 434 (2024) 139997-140008. https://doi.org/10.1016/j.jclepro.2023.139997